Prediction of Sedimentation and Consolidation of Fine Tails

William F. Eckert, Jacob H. Masliyah, Murray R. Gray, and Phillip M. Fedorak
Dept. of Chemical Engineering, University of Alberta, Edmonton, AB, Canada T6G 2G6

Sedimentation and consolidation of suspensions of fine particles were analyzed by integrating experimental measurement of properties in a centrifuge with a comprehensive numerical model. The yield stress and settling velocity for tailings from tar sands extraction were determined experimentally as a function of the volume fraction of solids. The evaluated state functions were used to simulate batch settling and consolidation, and the results compare well with long-term settling tube tests. This approach is very attractive where gravity sedimentation may take many years, and it allows prediction of the rate of clear water production, total time for sedimentation and consolidation, and the maximum concentration of solids.

Scaling of the sedimentation between centrifuge and field conditions is discussed. Conversion of permeability-void ratio relationships from geotechnical experiments to state functions of hindered settling velocity is demonstrated, allowing the use of data derived from a variety of experimental techniques.

Introduction

The effluent from most mineral recovery processes contains finely divided solids that tend to settle very slowly, and the resultant sediment has a very low solids content. Usually the effluent, or tailings stream, is directed to a tailings pond where settling of the solids and consolidation of the sediment take place. Due to environmental concerns, most of these processes are designed to be closed-loop systems, to minimize contamination of surface water. Fast settling solids that quickly produce a reusable clear water layer within a tailings pond are desirable, and therefore, the ability to predict the rate of clear water production for a particular tailings process is vital. Knowledge of the final consolidated concentration of sediment is also important for the estimation of the lifetime of a pond, and its potential for land reclamation.

Sedimentation of a suspension of solids will depend on the particle size, density, and surface properties. First, consider an ideal suspension undergoing batch settling, with an initial uniform suspension of hard spherical particles of 1 mm diameter. In this case, the suspension does not have any yield strength and quickly settles, so that all the particles form a sediment layer close to its maximum packing density. When settling has ceased, the system consists of a clear layer of liquid over a sediment layer.

Now consider batch settling of a suspension containing a low volume fraction of colloidal particles, as illustrated in Figure 1a. When particle size is of, say, less than 10 μm, attractive forces such as London–van der Waals forces become important and the particles can interact, forming flocs in suspension. The flocs may form a loose volume-filling network that has the ability to transmit stress. The threshold concentration at which the network forms is known as the gel point. If the stress applied to the network by the buoyed weight of the particles is greater than the corresponding strength of the network, it collapses to a higher concentration that can support the applied stress. The collapse occurs at the bottom of the suspension column, forming a bed of sediment. This bed will build upward over time and become a consolidated sediment layer or "soil." A clear layer of liquid forms at the column top with a sharp interface between the liquid and the initial suspension. The described deposition and consolidation process has been observed experimentally by Michaels and Bolger (1962), and Been and Sills (1981). The volume fraction of solids in the sediment varies with depth, from the original volume fraction (ϕ_o) at the suspension–sediment interface to a maximum value at the bottom of the column. Correspondingly, the compressive strength of

Correspondence concerning this article should be addressed to J. H. Masliyah.
Additional address of P. M. Fedorak: Dept. of Biological Sciences, University of Alberta, Edmonton, AB, Canada T6G 2E9.

the sediment layer is a function of the volume fraction of solids, and therefore the strength of the sediment also varies throughout its depth. When batch settling first starts, the suspension undergoes hindered settling with a velocity that is dependent on the hydrodynamics of the network of particles. As particles are deposited in the sediment layer at the bottom of the settling column, the depth of the uniform suspension decreases, while the depth of the sediment increases (Figure 1b). As the two interfaces approach each other a transition occurs between the hindered settling velocity of the suspension and the long-term consolidation velocity of the sediment. Eventually, the suspension layer becomes very shallow and sedimentation ceases. The sediment layer may consolidate further under its own weight; however, the amount of consolidation is usually small and occurs over a long time span. When the system has reached equilibrium, it consists of a layer of clear supernatant, a very thin layer of uniform suspension, and a bed of consolidated sediment or soil (Figure 1c). At this stage, the forces in the sediment are balanced by the compressive strength of the network. That is, at any depth in the sediment bed, the load due to the buoyed weight of the particles above is equal to the yield strength of the network at the corresponding volume fraction. The sediment layer has reached the maximum degree of consolidation possible for the prevailing stress, and could only be further consolidated by increasing the compressive load on the system, perhaps by applying a layer of material on top of the sediment.

In order to model the sedimentation and consolidation processes, the change in properties of the sediment with time must be taken into account. Two approaches to modeling have emerged, one from geotechnical engineering with a focus on the ability of sediments to support loads, and a second from the viewpoint of fluid dynamics.

Gibson et al. (1967) introduced a one-dimensional consolidation model for saturated clays that incorporated finite strain; that is, was not limited to small strains. They allowed for the variation in the compressibility and permeability of the soil during consolidation, and used Darcy's law in a form in which the relative velocity between the clay and pore fluid was used. The method of Gibson et al. has become the basis for the prediction of finite strain consolidation of water-saturated soils in the geotechnical and soil mechanics areas. However, the main concern of the geotechnical area has been the performance of a soil layer under an external load, and therefore rates of settlement and deposition have not been considered. The formulation is Lagrangian, that is, a material coordinate system is used, and therefore the upper boundary of the sediment is the coordinate origin, and a moving boundary problem need not be solved.

Buscall and White (1987) approached the problem from a fluid dynamics point of view, and developed a mathematical formulation to represent the settling and consolidation process. They introduced a modification to Kynch's equation (Kynch, 1952) for hindered settling by including the effect of the compressive strength of the suspension. Thus two state functions, yield strength and hindered settling velocity of the sediment, must be defined in order to fully characterize the settling and consolidation processes. In the same article, Buscall and White discussed a centrifugation technique for evaluating the compressive yield strength and the hindered settling rate of the solid suspension as functions of volume fraction. However, in order to define the volume concentration of solids at any location in the column, additional governing equations are needed. Auzerais et al. (1988) developed those two equations, which specify the movement of the clear fluid–suspension interface and the suspension–sediment interface.

In the present article, we have combined the experimental techniques of Buscall and White for the evaluation of the state functions with the theoretical formulation by Auzerais et al. This study demonstrates the use of centrifuge tests to evaluate the state functions of fine tails generated by the extraction of bitumen from the Athabasca tar sands and the prediction of the sedimentation and consolidation of these fines. In addition, the formulation of Auzerais et al. is applied to suspensions of saturated clay and copper concentrator fines, and it is found to successfully predict the solids concentration profile in the sediment layer and the total time for sedimentation and consolidation. The similarity of the one-dimensional finite strain equation of Gibson et al. to the governing equation of consolidation of Auzerais et al. is also demonstrated.

Mathematical Formulation

Consolidation governing equation

In the absence of inertia, a horizontal element of a particle network in a fluid is subject to three forces, as shown in Figure 2: (1) that due to hydrostatic pressure; (2) the buoyed

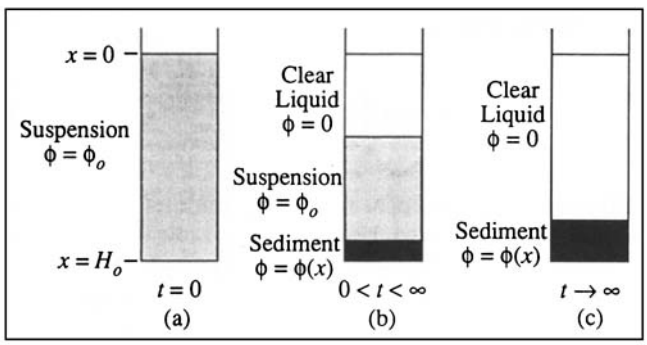

Figure 1. Nonideal batch system undergoing settling over time: (a) initial state; (b) intermediate state; (c) final state.

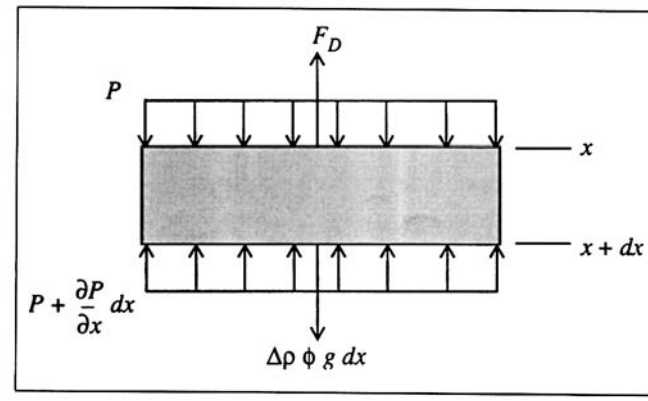

Figure 2. Forces acting on an element of a particle network.

weight, and (3) the hydrodynamic drag of the particles moving in the fluid. The hydrodynamic drag force of the network, F_D, is related to the drag force on a given particle, and includes the effect of particle concentration and the relative velocity between the particles and the liquid. The force balance equation for a horizontal element with a uniform cross-sectional area can be written as

$$-\frac{\partial P}{\partial x}+(\rho_s-\rho_f)g\phi-\frac{\lambda_{st}a_p\mu\phi r(\phi)}{V_p}(u_s-u_f)=0, \quad (1)$$

where P is the pressure or stress applied to the network, x is the vertical coordinate of the element measured from the top of the original suspension, ρ_s and ρ_f are the solid and fluid mass densities, g is the acceleration of gravity, ϕ is the volume fraction or concentration of the solids, λ_{st} is Stokes' drag coefficient for a single particle (equal to 6π for a sphere), a_p is the characteristic dimension of a particle (equal to the radius for a sphere), μ is the dynamic viscosity of the liquid, $r(\phi)$ is the hydrodynamic interaction function introduced by Buscall and White, V_p is the particle volume, and u_s and u_f are the velocities of the particles and fluid relative to an inertial frame of reference. The first term of Eq. 1 represents the applied pressure gradient on the network element in the vertical direction, the second term is the buoyed or submerged weight, and the third term is the hydrodynamic drag acting on the network. The density difference between the solids and the fluid will be given as $\Delta\rho$.

The continuity equation for the solids within the differential element is given by

$$\frac{\partial\phi}{\partial t}+\frac{\partial}{\partial x}[\phi u_s]=0, \quad (2)$$

where t represents time. The corresponding continuity equation for the fluid is given by

$$\frac{\partial(1-\phi)}{\partial t}+\frac{\partial}{\partial x}[(1-\phi)u_f]=0. \quad (3)$$

For batch settling or consolidation in a closed system, mass conservation of an incompressible liquid and solid dictates that

$$u_s\phi+u_f(1-\phi)=0. \quad (4)$$

Solving Eq. 4 for the fluid velocity results in

$$u_f=-\frac{u_s\phi}{(1-\phi)}. \quad (5)$$

Substituting the relationship for the velocity, u_f, from Eq. 5 into the force balance equation, Eq. 1, results in

$$-\frac{\partial P}{\partial x}+\Delta\rho g\phi-\frac{\Delta\rho g\phi r(\phi)}{U_\infty(1-\phi)}u_s=0, \quad (6)$$

where U_∞ is Stokes' single-particle settling velocity and is given by $U_\infty=\Delta\rho g V_p/\lambda_{st}\mu a_p$.

The hindered settling velocity of the suspension may be written as

$$U(\phi)=\frac{U_\infty(1-\phi)}{r(\phi)}. \quad (7)$$

Substituting for the hindered settling velocity, Eq. 7, into the force balance equation, Eq. 6, yields

$$-\frac{\partial P}{\partial x}+\Delta\rho g\phi-\frac{\Delta\rho g\phi}{U(\phi)}u_s=0. \quad (8)$$

Equation 8 can be rearranged to solve for the particle velocity to give

$$u_s=U(\phi)\left(1-\frac{1}{\Delta\rho g\phi}\frac{\partial P}{\partial x}\right). \quad (9)$$

Equation 9 is valid at any point in the suspension or sediment, and the particle velocity is not only dependent on the hindered settling relationship, but on the applied pressure gradient as well. In the initial state, the system consists of a suspension having a uniform volume fraction, and the pressure gradient is small. Therefore, the particle velocity will be essentially equal to the hindered settling velocity.

In the *consolidating sediment*, the applied pressure exceeds the yield stress of the network at the original volume fraction, and the network collapses to a denser concentration that has sufficient strength to carry the applied load. Therefore, the actual stress carried by the consolidating network is equal to the compressive yield stress corresponding to the local volume fraction. The yield stress itself is assumed to be dependent only on the volume fraction of the network at a particular location in the sediment. Hence, the applied pressure gradient in Eq. 9 can be replaced by the gradient of the compressive yield stress, P_y, resulting in

$$\frac{\partial P}{\partial x}=\frac{\partial P_y}{\partial x}=\frac{dP_y}{d\phi}\frac{\partial\phi}{\partial x}. \quad (10)$$

Combining Eqs. 9 and 10 gives the particle velocity in the consolidating layer as

$$u_s=U(\phi)\left(1-\frac{dP_y/d\phi}{\Delta\rho g\phi}\frac{\partial\phi}{\partial x}\right). \quad (11)$$

In the consolidating sediment layer, a significant volume fraction gradient exists, and the yield stress gradient term in Eq. 11 is large enough to greatly reduce the particle velocity.

Substituting the expression for the particle velocity, Eq. 11, into the solids continuity equation, Eq. 2, gives

$$\frac{\partial\phi}{\partial t}+\frac{\partial}{\partial x}\left[U(\phi)\left(\phi-\frac{dP_y/d\phi}{\Delta\rho g}\frac{\partial\phi}{\partial x}\right)\right]=0. \quad (12)$$

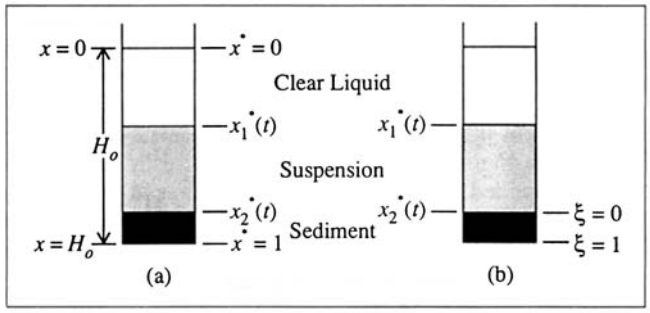

Figure 3. Transformation from (a) spatial to dimensionless coordinate; (b) dimensionless to nonmoving boundary coordinate.

This result is a modification of Kynch's equation for sedimentation, as given by Auzerais et al., allowing for the ability of a network to carry a load. If the network has no strength, that is, $P_y = 0$, then Eq. 12 simply reverts to Kynch's equation. Equation 12 contains two state functions, namely $U(\phi)$ and $P_y(\phi)$, which must be determined for a particular system before a solution can be achieved. In order to proceed with the solution of Eq. 12, two additional equations are required to unambiguously locate the interfaces.

Method of solution

Auzerais et al. introduced the necessary equations to locate the interfaces by first making Eq. 12 dimensionless through the introduction of the variables $x^* = x/H_o$, $t^* = tU_\infty/H_o$, and $U^*(\phi) = U(\phi)/U_\infty$, where H_o is the original suspension height. The new spatial coordinate has the range, $0 \le x^* \le 1$, which spans the original suspension height, with the upper interface between the clear fluid and suspension denoted as $x^*(t^*) = x_1^*(t^*)$, while the lower interface between the suspension and sediment layer is denoted as $x^*(t^*) = x_2^*(t^*)$, as shown in Figure 3a. Rewriting Eq. 12 in terms of the dimensionless variables gives the governing equation for consolidation

$$\frac{\partial \phi}{\partial t^*} + \frac{\partial}{\partial x^*}\left[U^*(\phi)\left(\phi - \frac{dP_y/d\phi}{\Delta \rho g H_o}\frac{\partial \phi}{\partial x^*}\right)\right] = 0. \quad (13)$$

Additional equations are needed to allow for the solution of the problem. They are the velocities of the clear liquid–suspension interface, x_1^*, and the suspension–sediment layer interface, x_2^*. The velocity of the x_1^* interface is found by first introducing the dimensionless variables into Eq. 9, which applies to both suspension and sediment layers, that is,

$$u_s^* = U^*(\phi_o)\left(1 - \frac{1}{\Delta \rho g H_o \phi_o}\frac{\partial P}{\partial x^*}\right). \quad (14)$$

Now, the pressure gradient term, $\partial P/\partial x$, in Eq. 14 needs to be defined. A linear variation in the applied stress is assumed in the suspension layer, with the applied network pressure at the x_1^* interface being zero, and at the x_2^* interface being the yield stress evaluated at $\phi = \phi_o$, giving

$$\frac{\partial P}{\partial x^*} = \frac{P_y(\phi_o)}{(x_2^* - x_1^*)}. \quad (15)$$

Finally, substituting Eq. 15 into 14 gives the velocity of the x_1^* interface as

$$\frac{dx_1^*}{dt^*} = U^*(\phi_o)\left[1 - \frac{1}{\Delta \rho g H_o \phi_o}\frac{P_y(\phi_o)}{[x_2^*(t) - x_1^*(t)]}\right]. \quad (16)$$

The velocity of x_2^* is found by examining the volume fraction at the top of the sediment layer. The volume fraction in the consolidating sediment is generally a function of position and time, but at x_2^* the volume fraction must be equal to the original volume fraction of the suspension, that is, $\phi(x_2^*, t^*) = \phi_o$. Therefore, the total differential of the volume fraction at top of the sediment is given by

$$\left[\frac{\partial \phi}{\partial x^*}dx^*\right]_{x^* = x_2^*} + \left[\frac{\partial \phi}{\partial t^*}dt^*\right]_{x^* = x_2^*} = 0. \quad (17)$$

Rearranging Eq. 17 gives the velocity of the x_2^* interface as

$$\frac{dx_2^*}{dt^*} = -\frac{\partial \phi/\partial t^*|_{x^* = x_2^*}}{\partial \phi/\partial x^*|_{x^* = x_2^*}}. \quad (18)$$

Equations 13 and 18 are combined to obtain the velocity of the x_2^* interface as

$$\frac{dx_2^*}{dt^*} = \frac{\dfrac{\partial}{\partial x^*}\left[U^*(\phi)\left(\phi - \dfrac{dP_y/d\phi}{\Delta \rho g H_o}\dfrac{\partial \phi}{\partial x^*}\right)\right]_{x^* = x_2^*}}{\left(\dfrac{\partial \phi}{\partial x^*}\right)_{x^* = x_2^*}}. \quad (19)$$

Equations 16 and 19 describe the motion of the boundaries of the settling and consolidating phases, and together with Eq. 13 form a system of equations for settling and consolidation of flocculating solids in a liquid. With an initial condition and two boundary conditions, they can be solved to yield the solids concentration profile of the entire column at any time, t^*.

In order to make the problem amenable to solution, Auzerais et al. introduced a transformation that reduced the moving boundary problem to one with a nonmoving boundary. The domain of the solution becomes $0 \le \xi \le 1$, where the moving boundary x_2^* is represented by $\xi = 0$, while $\xi = 1$ represents the fixed bottom of the column as shown in Figure 3b. The dimensionless coordinate is given by

$$\xi(t^*) = \frac{x^*(t^*) - x_2^*(t^*)}{1 - x_2^*(t^*)}. \quad (20)$$

Applying Eq. 20 to Eqs. 13, 16, and 19 results in the following governing equations for settling/consolidation:

$$\frac{\partial \phi}{\partial t^*} + \frac{(\xi - 1)}{(1 - x_2^*)} \frac{dx_2^*}{dt^*} \frac{\partial \phi}{\partial \xi} + \frac{1}{(1 - x_2^*)} \frac{\partial}{\partial \xi} \times \left[U^*(\phi) \left(\phi - \frac{1}{(1 - x_2^*)} \frac{dP_y/d\phi}{\Delta \rho g H_o} \frac{\partial \phi}{\partial \xi} \right) \right] = 0, \quad (21)$$

$$\frac{dx_1^*}{dt^*} = U^*(\phi_o) \left[1 - \frac{1}{(x_2^* - x_1^*)} \frac{P_y(\phi_o)}{\Delta \rho g H_o \phi_o} \right], \quad (22)$$

and

$$\frac{dx_2^*}{dt^*} = \frac{\frac{\partial}{\partial \xi} \left[U^*(\phi) \left(\phi - \frac{1}{(1 - x_2^*)} \frac{dP_y/d\phi}{\Delta \rho g H_o} \frac{\partial \phi}{\partial \xi} \right) \right]_{\xi = 0}}{\left(\frac{\partial \phi}{\partial \xi} \right)_{\xi = 0}}. \quad (23)$$

The preceding equations are solved by applying Eq. 21 to the consolidating sediment layer and integrating Eqs. 22 and 23 at every time step to locate the interfaces.

Equations 21–23 are subject to boundary conditions at the upper and lower surfaces of the consolidating sediment layer. First, at the upper boundary, $\xi = 0$, continuity of the volume fraction requires that $\phi(x_2^*, t^*) = \phi_o$. Also, the particle flux leaving the suspension layer must equal the particle flux entering the sediment layer. Since the flux is the product of the local particle velocity and the local volume fraction, we can write

$$\frac{dx_1^*}{dt^*} \phi_o = U^*(\phi_o) \left[1 - \frac{1}{(1 - x_2^*)} \frac{(dP_y/d\phi)_{\phi = \phi_o}}{\Delta \rho g H_o \phi_o} \left(\frac{\partial \phi}{\partial \xi} \right)_{\xi = 0} \right] \phi_o. \quad (24)$$

Equations 22 and 24 are combined to give the boundary condition at $\xi = 0$ as

$$\left(\frac{\partial \phi}{\partial \xi} \right)_{\xi = 0} = \frac{(1 - x_2^*)}{(x_2^* - x_1^*)} \frac{P_y(\phi_o)}{(dP_y/d\phi)_{\phi = \phi_o}}. \quad (25)$$

At the column bottom, $\xi = 1$, there can be no particle flux. This condition requires that the local particle velocity, u_s^*, be equal to zero, and we therefore write

$$\left[U^*(\phi) \left(1 - \frac{1}{(1 - x_2^*)} \frac{dP_y/d\phi}{\Delta \rho g H_o \phi} \frac{\partial \phi}{\partial \xi} \right) \right]_{\xi = 1} = 0. \quad (26)$$

Equation 26 can be rearranged to give the boundary condition at $\xi = 1$ as

$$\left(\frac{\partial \phi}{\partial \xi} \right)_{\xi = 1} = \left[\frac{(1 - x_2^*) \Delta \rho g H_o \phi}{dP_y/d\phi} \right]_{\xi = 1}. \quad (27)$$

We found that because of the high volume fraction gradient at the upper boundary of the sediment layer, the discretization of the sediment layer into a uniform grid required the use of a very fine grid spacing and a correspondingly small time step. The required CPU time for solution using a uniform grid was unacceptably long. Because the volume fraction gradient at the suspension–sediment interface required a very fine spatial grid to achieve a numerically stable solution, we applied an additional transformation to the solution space. This converted the uniform grid spacing to a stretched grid, where the grid spacing was fine near the $\xi = 0$ sediment boundary, and coarse at the $\xi = 1$ sediment boundary. The transformation is given by

$$\bar{\xi} = 1 - \frac{\ln([\beta + 1 - \xi]/[\beta - 1 + \xi])}{\ln[(\beta + 1)/(\beta - 1)]}, \quad (28)$$

which results in

$$\frac{\partial \bar{\xi}}{\partial \xi} = \frac{2\beta}{(\beta^2 - [1 - \xi]^2) \ln[(\beta + 1)/(\beta - 1)]}, \quad (29)$$

where the parameter β controls the degree of grid stretching. As β approaches 1, more of the grid is packed near the x_2^* boundary ($\xi = 0$), and as β nears infinity, the grid spacing becomes nearly uniform. The transformation allows the solution of the equations with a uniform grid spacing in the $\bar{\xi}$ domain.

In this article, the modeling of batch settling was done by applying Eq. 21 to the consolidating zone. The equation was discretized using an implicit method with a forward difference for the time derivative of ϕ and a central difference for the spatial derivatives of ϕ. This resulted in a tridiagonal system of equations with the coefficients being calculated from the previous time step. After solving for ϕ each node at the next time step, Eqs. 22 and 23 were integrated to give the new locations of x_1^* and x_2^*. The process was then repeated for each time step. A value of $\beta = 1.01$ gave a stable solution using few overall grid divisions and a reasonable time step, and was used for all the results shown in this article. A grid spacing of $\Delta \bar{\xi} = 1 \times 10^{-2}$, and a time step of $\Delta t^* = 1 \times 10^{-6}$ were also used.

An alternative solution scheme has been proposed by Howells et al. (1990), that discretizes the equations in time, then uses a Runge–Kutta shooting method to solve for the volume fraction profiles and the interface locations at each time step.

Comparison with the geotechnical formulation

Transformation of the Gibson et al. Lagrangian formulation, as used in the soil mechanics field, to Eq. 12 will be demonstrated. The finite strain equation for one-dimensional consolidation of saturated clays as given by Gibson et al. is

$$\pm \left(\frac{\gamma_s}{\gamma_f} - 1 \right) \frac{d}{de} \left[\frac{k(e)}{1 + e} \right] \frac{\partial e}{\partial z} + \frac{\partial}{\partial z} \left[\frac{k(e)}{\gamma_f (1 + e)} \frac{d\sigma'}{de} \frac{\partial e}{\partial z} \right] + \frac{\partial e}{\partial t} = 0, \quad (30)$$

where the negative sign is used when z is measured with gravity, k is the permeability of the sediment, e is the void ratio, γ_f and γ_s are the fluid and particle weight densities, and σ' is the effective stress applied to the network. The Gibson et al. equation is a Lagrangian formulation with z representing the material coordinate, while the fluid dynamics equations given previously are based on the spatial coordinate x. For a given value of z, the mass of the solids between that location and the bottom of the particle column is a constant. For example, if the value z locates the half-height position in the original uniform suspension, then any time thereafter that value of z would locate the position in the suspension or sediment where half the particle mass is below it.

First, Eq. 30 is converted from a material coordinate system to a spatial coordinate system. At a given time, the relationship between the material coordinate, z, and the spatial coordinate, x, is dependent only on the porosity or void fraction of the solids between z and the bottom of the column, and is given by

$$x(z) = \int_0^z (1+e)\,dz, \tag{31}$$

and the derivative of x yields

$$\frac{\partial x}{\partial z} = (1+e). \tag{32}$$

In Eq. 30 the void fraction, e, is a function of the material coordinate, z, and time, t. As shown by Been (1980), we may define a new void fraction, $\bar{e}$, that is a function of the spatial coordinate, $x(z,t)$, and time, t. The functional forms of e and $\bar{e}$ may differ; however, at a given position, z, and time, t, the values of the two void fractions must be equal, that is, $e(z,t) = \bar{e}[x(z,t),t]$. This results in the following relationship

$$\frac{\partial e}{\partial z} = \frac{\partial \bar{e}}{\partial x}\frac{\partial x}{\partial z}. \tag{33}$$

And since $\partial e/\partial t$ is a material or convective derivative, we may write

$$\frac{\partial e}{\partial t} = \frac{\partial \bar{e}}{\partial x}\frac{\partial x}{\partial t} + \frac{\partial \bar{e}}{\partial t}. \tag{34}$$

Combining Eqs. 32–34 with Eq. 30 gives the finite strain equation in terms of the spatial coordinate, x, as follows:

$$-\frac{\Delta\gamma}{\gamma_f}\frac{\partial}{\partial x}\left[\frac{k(\bar{e})}{1+\bar{e}}\right](1+\bar{e}) + (1+\bar{e})\frac{\partial}{\partial x}\left[\frac{k(\bar{e})}{\gamma_f}\frac{d\sigma'}{d\bar{e}}\frac{\partial \bar{e}}{\partial x}\right] + \frac{\partial \bar{e}}{\partial x}\frac{\partial x}{\partial t} + \frac{\partial \bar{e}}{\partial t} = 0, \tag{35}$$

where $\Delta\gamma$ is the difference between the solid and fluid weight densities.

Before we can complete the transformation, the relationships between ϕ and $\bar{e}$, and between $U(\phi)$ and $k(\bar{e})$ must be known. First, the relationship between volume fraction, ϕ, and void ratio, $\bar{e}$, is given by

$$\phi = \frac{1}{1+\bar{e}}. \tag{36}$$

Equation 36 also gives

$$\frac{\partial \bar{e}}{\partial \phi} = -\frac{1}{\phi^2} \tag{37}$$

and

$$d\bar{e} = -\frac{1}{\phi^2}\,d\phi. \tag{38}$$

We can write that

$$\frac{\partial \bar{e}}{\partial x} = \frac{\partial \bar{e}}{\partial \phi}\frac{\partial \phi}{\partial x} \tag{39}$$

and

$$\frac{\partial \bar{e}}{\partial t} = \frac{\partial \bar{e}}{\partial \phi}\frac{\partial \phi}{\partial t}. \tag{40}$$

Second, Darcy's law can be expressed in terms of the difference between the fluid and solids velocities, as

$$(1-\phi)(u_f - u_s) = -\frac{k}{\gamma_f}\frac{\partial p}{\partial x}, \tag{41}$$

where p is the excess pore pressure. The constant k is commonly referred to as the permeability. However, in this form it has units of velocity and is more properly termed the hydraulic conductivity. Applying Eq. 5, which relates the solid and fluid velocities in a batch settling column, and solving for the pressure gradient by rearranging Eq. 41, allows Darcy's law to be written as

$$\frac{\partial p}{\partial x} = \frac{u_s \gamma_f}{k}. \tag{42}$$

Equation 42 is the excess pore pressure gradient due to the hydrodynamic drag of the relative motion of the particles to the fluid, which must be equal to the hydrodynamic drag term of Eq. 8. Equating these two drag terms results in the desired relationship between the permeability and hindered settling velocity, that is,

$$U(\phi) = \frac{k\Delta\gamma\phi}{\gamma_f}. \tag{43}$$

Also, the partial derivative of x with respect to time is equal to the particle velocity in the consolidating layer, u_s, giving

$$\frac{\partial x}{\partial t} = U(\phi)\left(1 - \frac{dP_y/d\phi}{\Delta\rho g\phi}\frac{\partial \phi}{\partial x}\right). \tag{44}$$

Combining Eqs. 36–40, and Eqs. 43 and 44 with Eq. 35 gives

$$\phi\frac{\partial}{\partial x}[U(\phi)]-\phi\frac{\partial}{\partial x}\left[\frac{U(\phi)}{\Delta\gamma\phi}\frac{d\sigma'}{d\phi}\frac{\partial\phi}{\partial x}\right]+\frac{\partial\phi}{\partial x}\left[U(\phi)\left(1-\frac{dP_y/d\phi}{\Delta\rho g\phi}\frac{d\phi}{dx}\right)\right]+\frac{\partial\phi}{\partial t}=0. \quad (45)$$

Finally, recalling that $\Delta\gamma=\Delta\rho g$, and that in the consolidating layer the effective stress, σ', is equal to the yield stress, P_y, allows Eq. 45 to be simplified to

$$\frac{\partial\phi}{\partial t}+\frac{\partial}{\partial x}\left[U(\phi)\left(\phi-\frac{dP_y/d\phi}{\Delta\rho g}\frac{\partial\phi}{\partial x}\right)\right]=0. \quad (46)$$

Equation 46 is the same as the governing equation of consolidation as developed by Auzerais et al. (Eq. 12). Therefore, the fluid dynamics formulation for consolidation is the same as the one-dimensional finite strain equation of Gibson et al., using a different frame of reference. The suspension-hindered settling velocity, $U(\phi)$, accounts for variation in the permeability, $k(e)$, of the suspension network with respect to void ratio or volume fraction. The geotechnical formulation uses the effective stress acting on the suspension during consolidation, σ', whereas the fluid dynamics formulation uses the compressive yield stress, P_y.

Experimental Methods

The fine tails used for this study were produced by the hot water extraction of oil from Athabasca tar sands. Fifteen 55-gal (208-L) barrels of effluent were obtained, and the coarse solids were allowed to settle. The remaining fine tails were combined in a large tank, mixed by pumping, and then transferred to 55-gal (208-L) drums for storage. Four-liter stocks of tailings were taken from the barrels and filtered through a 106-μm sieve under a partial vacuum, resulting in samples of whole fine tails. The particle size distribution of the remaining solids in the whole fine tails is shown in Figure 4. Some

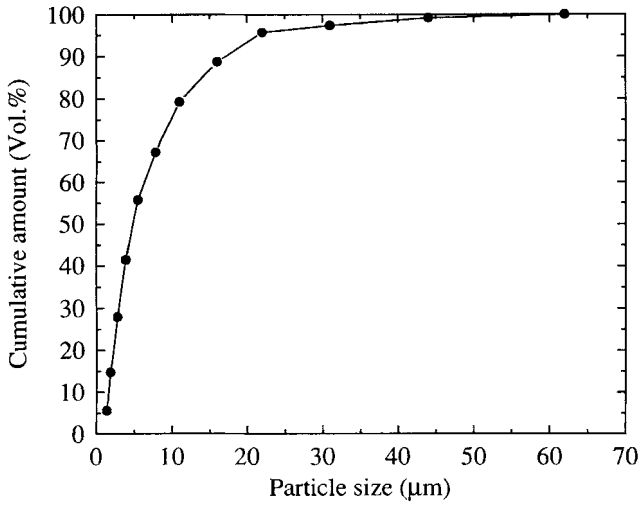

Figure 4. Particle size distribution of whole fine tails.

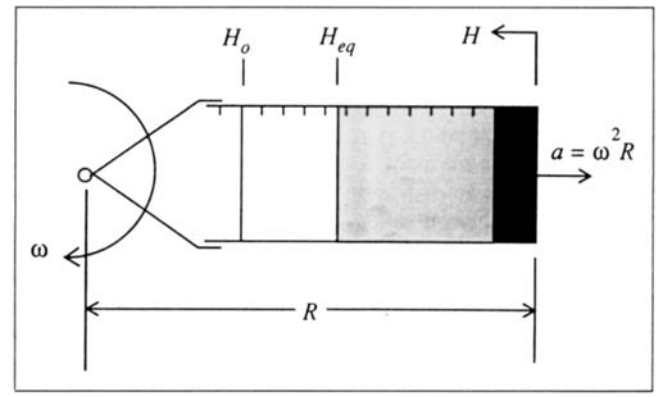

Figure 5. Flat-bottomed test tube in a centrifuge.

of the whole fine tails were further processed to remove bitumen. The tails were centrifuged at high speed to form a wet cake of solids, and bitumen was removed from the cake by Soxhlet extraction with toluene. The resulting solids were then resuspended in clear tailings water to produce bitumen-free tails with solids content from 10 to 40 wt. %. For complete details of the sample preparation process see Theriault et al. (1995).

The governing equation for consolidation, Eq. 12, requires two state functions, $P_y(\phi)$ and $U(\phi)$, as well as the densities of the solids and liquid. The state functions for the compressive yield strength of the network, $P_y(\phi)$, and the hindered settling velocity, $U(\phi)$, are both purely functions of the volume fraction of the solids for a given solids–fluid system. Suggested forms of these functions are (Auzerais et al.)

$$P_y=\frac{P_o\phi^n}{(c-\phi)} \quad (47)$$

and

$$U(\phi)=U_\infty(1-\phi)^m, \quad (48)$$

where P_o, c, n, U_∞, and m are found by curve fitting experimental data. U_∞ is Stokes' settling velocity for a single particle in an infinite fluid field. In this article, the experimental data needed to arrive at these functions were obtained from centrifuge testing of fine tails samples using the methods of Buscall and White, and as described below.

As shown in Figure 5, the angular velocity of a centrifuge creates an apparent centrifugal acceleration field to an observer moving with the test tube. The magnitude of the centrifugal acceleration, which varies with the radius from the center of rotation, increases the settling and consolidation rates, and thereby allows measurement to be done more quickly than when subjected to gravity alone.

To determine the variation of the compressive yield stress, P_y, with volume fraction, the applied compressive stress and the corresponding solids concentration at any given position in the sediment are needed. To achieve this, a sample of uniform suspension, with known initial volume fraction of solids, was subjected to a low initial centrifugal acceleration in a centrifuge. We used a low-speed purpose-built centrifuge with a transparent cover. The centrifuge tubes were illuminated

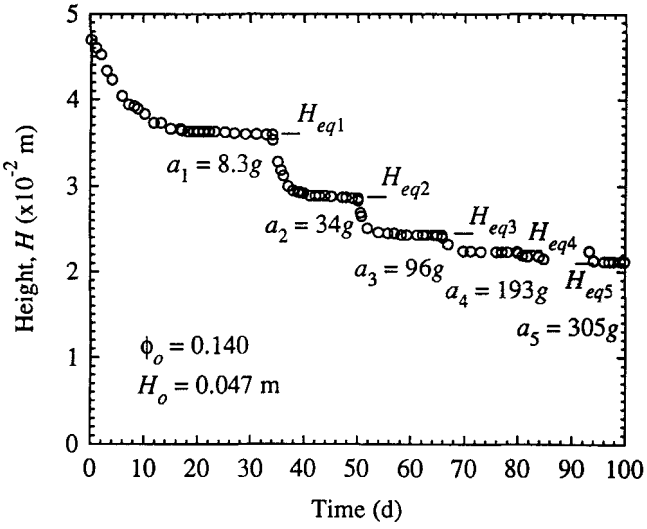

Figure 6. Suspension height vs. time for bitumen-free tails sample I (centrifuge test).

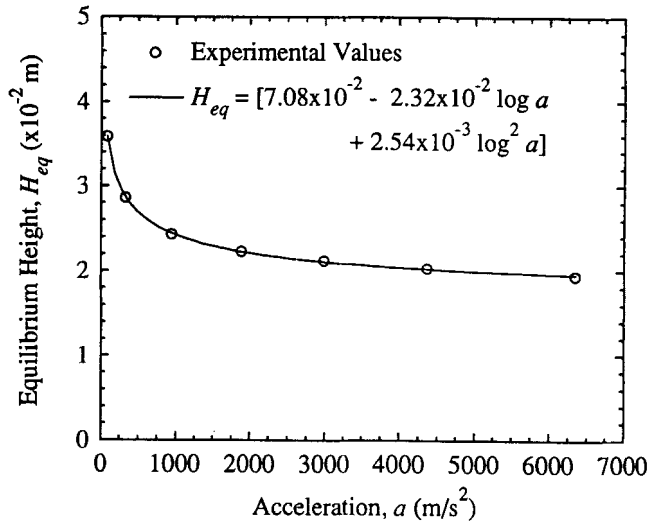

Figure 7. Equilibrium height to acceleration curve fit for sample I of bitumen-free tails.

by a stroboscope synchronized to the centrifuge rotational velocity, and the heights of the suspensions were measured using graduated test tubes. This method allowed height readings to be taken with the centrifuge running, thus eliminating any possible rebound of the interfaces. The height of the clear liquid–suspension interface was read periodically, with the height being measured upward from the tube bottom. The centrifuge speed, and hence centrifugal acceleration, was kept constant until the interface height reached equilibrium, that is, height remained constant over several days. This gave the equilibrium height, H_{eq}, of the fine tails sample for a known centrifugal acceleration at the tube bottom, a. The compressive stress at the test tube bottom, P_B, is related to H_{eq} by the approximate expression (Buscall and White, 1987)

$$P_B \approx \Delta\rho a \phi_o H_o \left(1 - \frac{H_{eq}}{2R}\right), \tag{49}$$

where H_o is the original height of the uniform suspension, and R is the radius to the bottom of the centrifuge tube. Equation 49 accounts for the radial variation in the centrifugal acceleration field, but assumes a uniform volume fraction suspension. The centrifuge speed was then increased in steps, with the interface height being allowed to reach equilibrium at each speed, giving a new applied compressive stress at each speed. An example of the resulting equilibrium height curve for sample I of bitumen-free tails is shown in Figure 6. The figure shows the equilibrium height for five different acceleration values, with the first centrifugal acceleration at tube bottom being equal to 8.3 times the acceleration of gravity.

The corresponding volume fractions at the test tube bottom were calculated from the approximation (Buscall and White, 1987)

$$\phi_B \approx \frac{\phi_o H_o \left[1 - \frac{1}{2R}\left(H_{eq} + a\frac{dH_{eq}}{da}\right)\right]}{\left[\left(H_{eq} + a\frac{dH_{eq}}{da}\right)\left(1 - \frac{H_{eq}}{R}\right) + \frac{H_{eq}^2}{2R}\right]}. \tag{50}$$

The derivative of the equilibrium height, H_{eq}, with respect to centrifugal acceleration, a, was evaluated from plots of H_{eq} vs. a. This was done by curve fitting the experimental H_{eq} to a, and then differentiating the resulting equation. The variation of equilibrium height with acceleration for sample I of bitumen-free tails is shown in Figure 7.

Because equilibrium was reached at each speed, the compressive yield strength can be equated to the calculated applied stress. Therefore, for each acceleration value used, the compressive yield stress, P_B, and the corresponding volume fraction at the tube bottom, ϕ_B, were known. The tests were replicated for three samples of bitumen-free tails. A plot of the experimental values of P_B and ϕ_B for each of the samples, and the average yield stress relationship, $P_y(\phi)$, for the bitumen-free tails is shown in Figure 8.

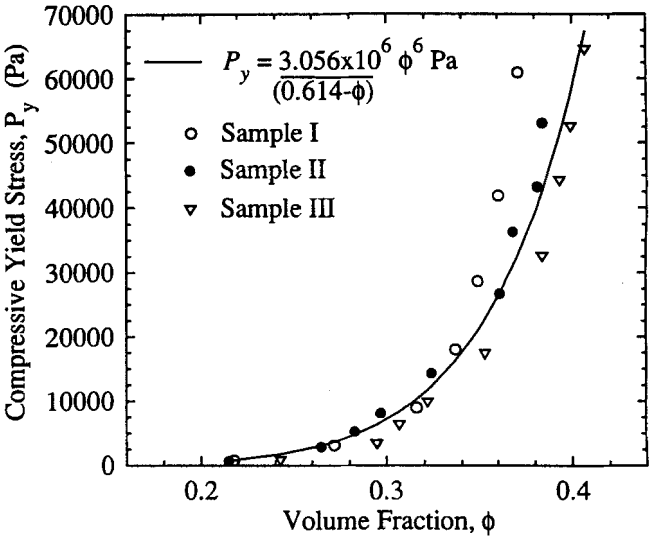

Figure 8. Compressive yield stress as a function of volume fraction, ϕ, for bitumen-free tails (centrifuge test).

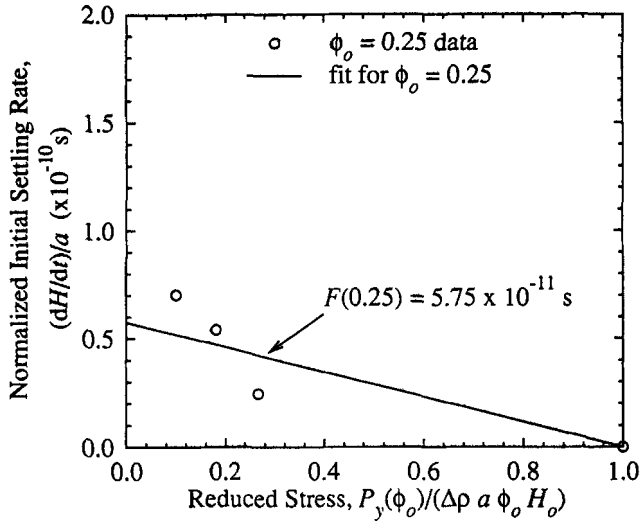

Figure 9. Variation of the normalized initial settling rate with the reduced stress for bitumen-free tails ($\phi_o = 0.25$).

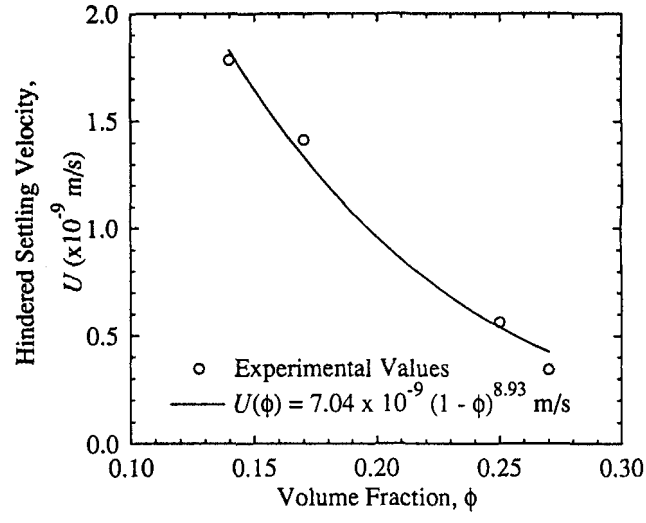

Figure 10. Hindered settling velocity, U, as a function of volume fraction, ϕ, for bitumen-free tails (centrifuge test).

A second state function, $U(\phi)$, the hindered settling velocity of the network, was also needed. The centrifuge was again used to provide the data needed to derive such a relationship. For a known initial volume fraction, the initial settling rate of the liquid–suspension interface was measured. This was repeated for several acceleration values, with the sediment being resuspended by gentle stirring and shaking before each run. Buscall and White found that the initial settling rate divided by the applied centrifugal acceleration has a linear relationship to a reduced yield stress term, that is,

$$-\frac{1}{a}\left[\frac{dH}{dt}\right]_{t=0} = F(\phi_o)\left(1 - \frac{P_y(\phi_o)}{\Delta\rho a \phi_o H_o}\right), \qquad (51)$$

where $F(\phi_o) = U(\phi_o)/a$, the reduced yield stress is $[P_y(\phi_o)/(\Delta\rho a \phi_o H_o)]$, and H is the liquid–suspension interface height measured from the centrifuge tube bottom. A plot of $-(1/a)(dH/dt)_{t=0}$ vs. the reduced stress results in a straight line for a given volume fraction where the intercept of the x-axis is unity. The slope of the resulting straight line gives the value of $F(\phi_o)$, and hence the hindered settling velocity, $U(\phi_o)$. The process was repeated for different initial volume fractions of the fine tails suspension, giving data for F, and thus U, vs. ϕ_o. An example of the relationship of the reduced stress to the normalized initial settling rate for bitumen-free tails with an initial volume fraction of 0.25, and the corresponding slope, $F(0.25)$, is shown in Figure 9. The hindered settling velocity as a function of volume fraction for the bitumen-free tails is shown in Figure 10, and assumes an applied acceleration equal to that of gravity.

Results and Discussion

The evaluated state functions for bitumen-free tails are shown in Figures 8 and 10, and were used in our modification of the Auzerais et al. equations to numerically reproduce the equilibrium height vs. time curve for sample I of bitumen-free tails. Figure 11 shows that the predicted supernatant–suspension interface, x_1^*, follows the experimental curve almost exactly. Also shown as a dotted line is the predicted suspension–sediment interface, x_2^*. It was not possible to determine the depth of the sediment bed with the experimental procedure employed, because this interface could not be visually detected. However, qualitatively the predicted interface does follow the growth of a sediment layer in a settling tube as observed by Been with an X-ray technique.

The question that naturally arises, is whether the numerical prediction of the originally measured equilibrium curves is not an elaborate circular method of curve fitting. It is true that the state functions were experimentally determined from such plots. It is also true that the hindered settling velocity function does determine the predicted initial settling velocity of the suspension, and that the compressive yield stress func-

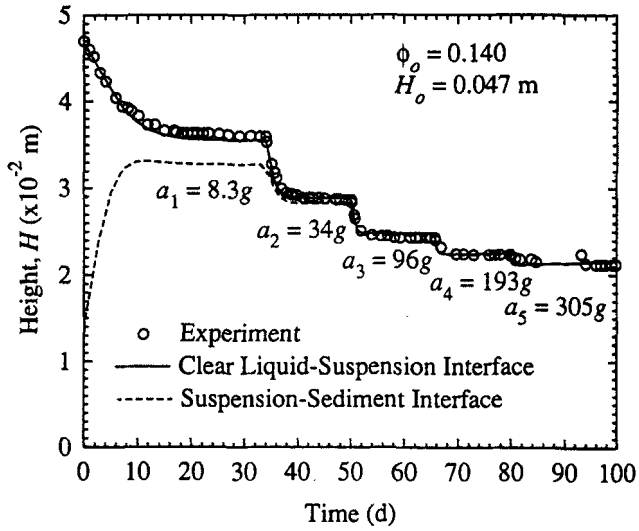

Figure 11. Measured suspension heights in a centrifuge vs. numerical prediction of both suspension and sediment layer heights for sample I of bitumen-free tails.

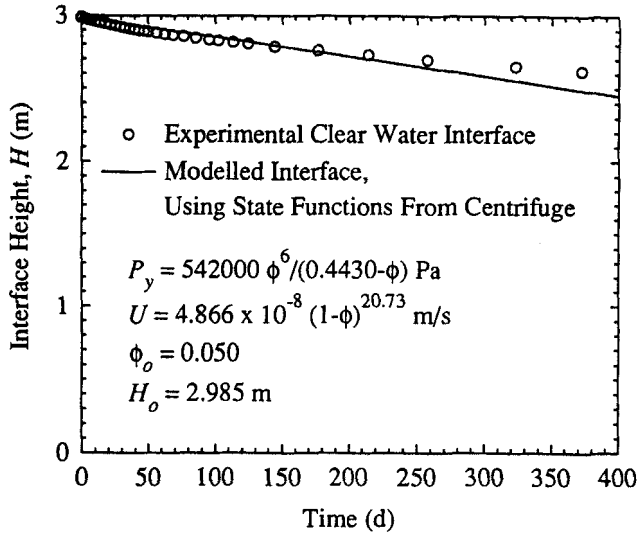

Figure 12. Measured height of interface in a settling tube vs. modeled height for whole fine tails.

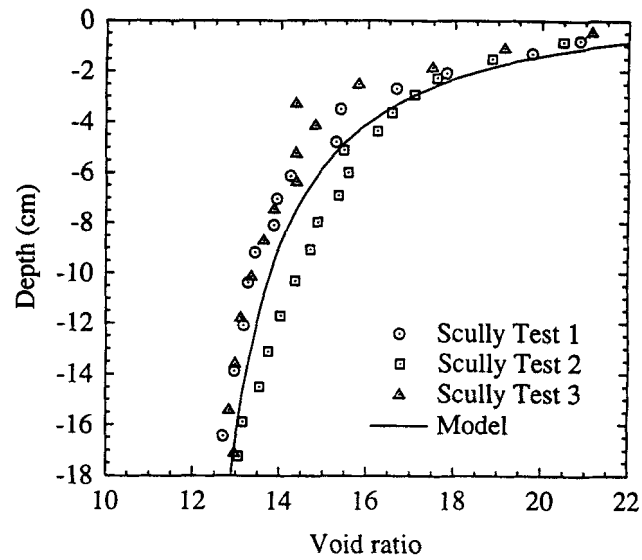

Figure 13. Density profile in the sediment layer of saturated clay from a settling tube test (Scully et al., 1984) with our numerical prediction.

tion determines the computed equilibrium height of the suspension. As can be seen in Figure 11, the predicted and measured initial settling rates and final equilibrium heights agree well. However, the transition curve between the initial region of hindered settling and the equilibrium height is governed by the consolidation equation (Eq. 12), and the fact that the numerical results match the experimental data so well, in this transition region, validates the method employed.

We also conducted concurrent settling tube tests and centrifuge tests on samples of whole fine tails. The resulting state functions for the whole tails were then used to model the settling tube tests numerically. A comparison of the measured height of the clear water–suspension interface in a settling tube vs. the predicted height is shown in Figure 12. The corresponding state functions for whole fine tails, as evaluated with centrifuge tests, are also given in Figure 12. The elapsed time of the experiment was just over one year, with the original suspension having a solids volume concentration of 5%, a height of 2.985 m, and a diameter of 0.0254 m. The predicted height of the interface follows the experimental height closely. The small discrepancy in the predicted vs. actual initial settling rate could be due to a wall effect in the settling tube. The wall effect is greater in a small-diameter tube, and effectively decreases the hindered settling velocity (see Michaels and Bolger, 1962). Larger diameter tubes would have decreased or eliminated this effect. The prediction or modeling of gravity settling for whole fine tails, such as used here, is an extreme extension of previous studies (Michaels and Bolger, 1962; Been and Sills, 1981) as typical times for complete sedimentation and consolidation of the present system measure not in months or years, but in centuries.

As an additional test, the numerical method was used when the state functions were determined by other techniques. Scully et al. (1984) presented experimental and numerical results for the settling of phosphatic clay in water at very high original void ratios, e. The void fraction profiles of the consolidated sediment layer in several settling tubes were presented, along with the effective stress–void ratio curves and the permeability–void ratio curves based on settling tube and constant rate of deformation tests. The effective stress–void ratio and permeability–void fraction curves were converted to compressive stress–volume fraction and hindered settling velocity–volume fraction data that were curve fit to relationships of the form of Eqs. 47 and 48. The settling tube experiments were then modeled using the newly derived state functions with the modified model of Auzerais et al. A comparison of the final predicted void ratio profile of the sediment layer and the experimentally measured is shown in Figure 13. Again, the numerical method gives excellent agreement with the experimental profile of void ratio from the settling tube. Scully et al. noted that the settling tests, which had an original height of 36 cm and a uniform void ratio of 30, were run for 8–12 days for complete consolidation. Our numerical model predicted equilibrium would be reached in approximately 5 days.

Bustos and Concha (1988) published studies simulating batch sedimentation of flocculated suspensions. They developed another method based on fluid dynamics principles, but noted that their equations were nonlinear and the resulting solutions were discontinuous, and introduced Rankine–Hugoniot or jump conditions to attain their solutions. Based on their experimental work, Bustos and Concha derived the following state functions for flocculated fine tails from a copper concentrator:

$$P_y = 5.35e^{17.9\phi}\ \text{N/m}^2, \tag{52}$$

$$U(\phi) = 6.05 \times 10^{-4}(1-\phi)^{12.59}\ \text{m/s}. \tag{53}$$

Making use of the state functions, we simulated the settling of copper fine tails in a batch settling tube, and compared our numerical predictions with those of Bustos and Concha as shown in Figure 14. The original volume fraction was 0.123, and the original height of fine tails was 0.405 m. The solids lines in Figure 14 represent our numerical predictions for the

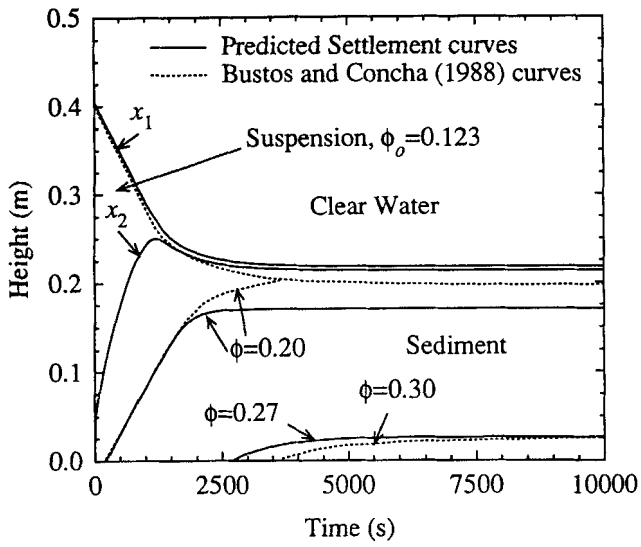

Figure 14. Predicted settling of fine tails from a copper concentrator: ours vs. Bustos and Concha's (1988).

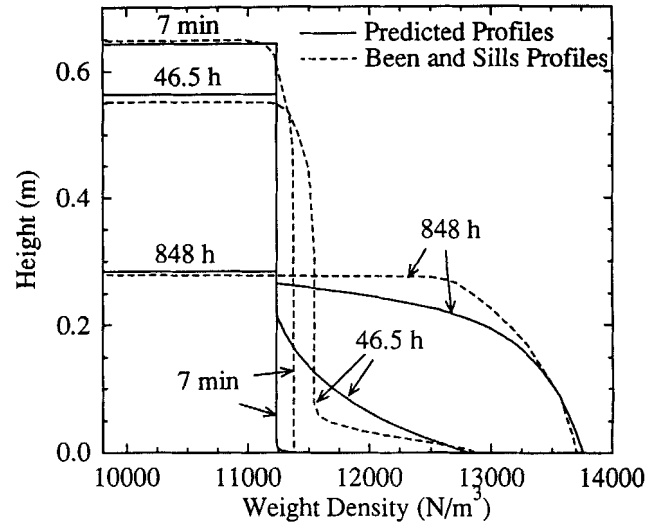

Figure 15. Density profiles for a suspension of clay in water: our prediction vs. those measured in experiment #15 by Been and Sills (1981).

height of the clear water–suspension interface, and the suspension–sediment interface along with lines of constant volume fraction for values of 0.20 and 0.27. The dotted lines represent the suspension surface height and lines of constant concentration for values of 0.20 and 0.30 as predicted by Bustos and Concha. Our prediction of the surface height was similar to the Bustos and Concha prediction for the initial constant rate settling period; however, our final consolidated height was approximately 10% higher. They noted that they had good agreement between experimental results and the predicted heights obtained from their simulation, but did not give the actual experimental values. Our predicted curve of the clear water–suspension interface is close to the Bustos and Concha simulation. The Bustos and Concha prediction, for the isoline of $\phi = 0.20$, is the same as our predicted line in the initial phase. However, the Bustos and Concha prediction for the final height is slightly higher than that given by our simulation. Their simulation additionally gave an isoline of $\phi = 0.30$ near the bottom of the sediment layer that rises to meet our predicted isoline of 0.27. The sediment layer could not attain a consolidated volume fraction of 0.30 at the bottom based on the yield stress relationship provided. If one considers the total compressive stress on the sediment at equilibrium, which is merely equal to the buoyed weight of the total column of sediment, then the compressive yield stress relationship indicates that the corresponding volume fraction should be 0.275. In fact, our simulation predicted a maximum volume fraction of 0.275 at the bottom of the soil layer, and would appear to be more realistic on that basis. Qualitatively, our numerical method does produce similar results to that of Bustos and Concha (1988).

Been and Sills (1981) also gave results for batch settling of a clay–water suspension in 2-m settling tubes. In particular, we retrieved the data presented for experiment 15, and converted their effective stress–void ratio and permeability–void ratio relationships to corresponding state functions of $P_y(\phi)$ and $U(\phi)$. Figure 15 compares our predicted density profiles at several different times to those measured by Been and Sills. Note that the origin of the density scale is 9,800 N/m^3, which is the weight density of water, and the tube was originally filled with a suspension of a uniform weight density of 11,200 N/m^3. The predicted clear water–suspension interfaces at the 7-min, 46.5-h, and 848-h time intervals agree well with the measured values. The predicted densities at the bottom of the settling tube also agree well with the measured densities, although the density profiles in the sediment layer near the bottom show some differences. Our final predicted density profile at 848 h, when the sedimentation and consolidation had stopped, showed good agreement with the measured profile. However, the experimentally measured profiles show that the density and hence volume fraction in the suspension layer does not maintain a perfectly constant value. In fact, the measured density of the suspension layer did increase with depth after only a few minutes. The sedimentation and consolidation theory used in this study assumes that the volume fraction in the suspension layer remains uniform, and therefore cannot model the densification observed by Been and Sills. A recent paper by Shen et al. (1994) also observed consolidation throughout the suspension layer, rather than only at the location where the network stress exceeded the compressive yield stress. They theorized that a stress-induced creep mechanism may be responsible for the difference between the present consolidation theory and experimental observations.

Making use of the state functions for fine tails (see Figures 8 and 10), a field tailings pond was simulated as a batch system; with the pond being originally filled with a suspension of 7% volume concentration to a depth of 20 m. The field values are typical for tailings ponds in the tar sands industry. The clear water–suspension and suspension–sediment interface heights, as predicted over time, are shown in Figure 16. The predicted time for sedimentation was approximately 125 years, with self-weight consolidation taking another 25 years. The final predicted concentration of solids at the bottom of the sediment was 25% by volume or 58% by weight.

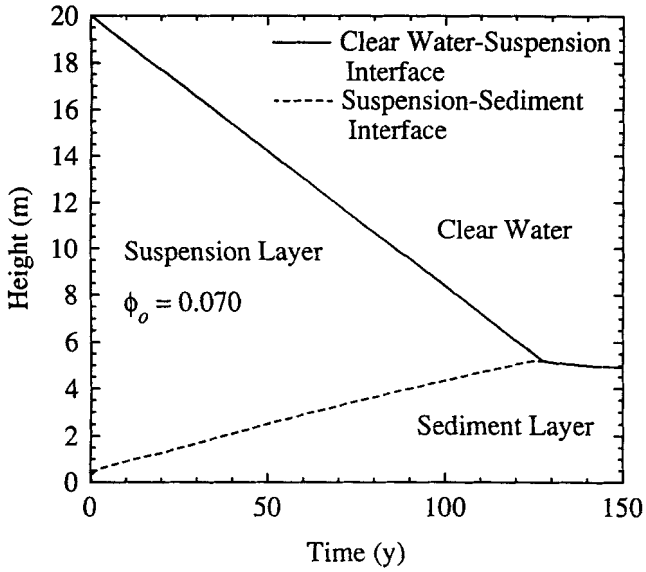

Figure 16. Predicted sedimentation and consolidation of a tailings pond based on the properties of bitumen-free tails as measured in a centrifuge (Figures 8 and 10).

Scaling

Using the governing equation for consolidation allows one to examine the effective scaling of the centrifuge tests. Equation 13 can be rewritten as

$$\frac{\partial \phi}{\partial t^*} + \frac{\partial}{\partial x^*}\left[U^*(\phi)\phi_o\left(\frac{\phi}{\phi_o} - \left[\frac{dP_y^*/d\phi}{Pe}\right]\frac{\partial \phi}{\partial x^*}\right)\right] = 0, \quad (54)$$

where P_y^* is the yield stress function normalized by P_o, a constant and characteristic value of the yield stress function as given by Eq. 47; and Pe is the Péclet number, which is the ratio of the compressive stress at the column bottom to P_o, and is given by

$$Pe = \frac{\Delta \rho a H_o \phi_o}{P_o}. \quad (55)$$

Recognizing that all the terms of Eq. 54 are dimensionless, then for a given fine tails suspension, the governing dimensionless group is given by the Péclet number.

Consider the case where the Péclet number is the same for the sample in the centrifuge as the fine tails in the field. We then have

$$\frac{\Delta \rho_F g H_{oF} \phi_{oF}}{P_{oF}} = \frac{\Delta \rho_C a_C H_{oC} \phi_{oC}}{P_{oC}}. \quad (56)$$

If the centrifuge sample contains the same material as the tailings pond, then the characteristic yield strength and the relative densities are the same, and the length scale is given by

$$\frac{H_{oF}}{H_{oC}} = \frac{a_C}{g}\frac{\phi_{oC}}{\phi_{oF}}. \quad (57)$$

If the field tailings pond depth is 20 m and the depth of the sample in the test tube is 0.05 m, then assuming equal original volume fractions, the centrifuge test would need to apply an acceleration field equal to $400g$ in order to simulate consolidation in the field. This level of centrifugal acceleration can easily be attained in laboratory centrifuges.

If we consider the time scaling between the centrifuge and the field, we need to consider the dimensionless time used in the model, leading to

$$\frac{t_F U_{\infty F}}{H_{oF}} = \frac{t_C U_{\infty C}}{H_{oC}}. \quad (58)$$

The ratio between the single-particle settling velocity in the centrifuge, $U_{\infty C}$, to that in the field, $U_{\infty F}$, is again the ratio of the acceleration in the centrifuge to the acceleration of gravity, and we can rewrite Eq. 58 as

$$\frac{t_F}{t_C} = \frac{a_C}{g}\frac{H_{oF}}{H_{oC}}. \quad (59)$$

Combining Eqs. 57 and 59 results in

$$\frac{t_F}{t_C} = \left(\frac{a_C}{g}\right)^2 \frac{\phi_{oC}}{\phi_{oF}}. \quad (60)$$

Again, if the original volume fractions of the centrifuge sample and the tailings pond are equal, then the scaling between the time taken in the field, and the elapsed time in the centrifuge test is the ratio of the applied centrifugal acceleration to the acceleration of gravity squared. So, at a modest centrifuge acceleration of $100g$, 0.9 h in the centrifuge would represent one year of consolidation in the field. Therefore, the centrifuge can be used to greatly accelerate the testing of consolidation of a fine tails produced under a given set of operating conditions.

Conclusions

Our results show the merits of combining centrifugal sedimentation experiments with a numerical model. The measured state functions, when used in the numerical model, are shown to agree well with batch-settling tests. For suspensions such as the bitumen-free tails and whole fine tails used in this work, settling tube tests often require years to provide meaningful results. A shorter-term method of evaluating the physical properties of the tails using a centrifuge and modeling the batch sedimentation process with the fluid dynamics equations appears from our results to be a viable alternative.

We have also shown that the governing equation for consolidation used in the soil mechanics area and the fluid dynamics equation are in fact the same equation formulated from a different frame of reference. The transformation of the permeability–void ratio relationship used in the soil mechanics field to a hindered settling velocity–volume fraction relationship was shown. State functions derived from other experimental techniques, such as settling tube tests or constant rate of deformation tests, can be used to model centrifuge experiments and behavior in the field.

Acknowledgments

The authors are grateful for the generosity of the Natural Sciences and Engineering Research Council of Canada that allowed this work to proceed. As well, thanks are extended to Syncrude Canada Ltd. for supplying samples and data, and for their continued support. Thanks are also due to Nancy Irwin for her initial work on the numerical model, and to Leanne Thompson for her experimental work.

Notation

c = constant in state equation $P_y = P_o \phi^n/(c - \phi)$
m = constant in state equation $U = U_\infty(1 - \phi)^m$
n = constant in state equation $P_y = P_o \phi^n/(c - \phi)$

Greek letters

$\bar{\xi}$ = stretched dimensionless coordinate
ω = angular velocity, rad/s

Literature Cited

Auzerais, F. M., R. Jackson, and W. B. Russel, "The Resolution of Shocks and the Effects of Compressible Sediments in Transient Settling," *J. Fluid Mech.*, **195**, 437 (1988).

Been, K., "Stress Strain Behaviour of a Cohesive Soil Deposited Under Water," PhD Thesis, Oxford Univ., Oxford (1980).

Been, K., and G. C. Sills, "Self-Weight Consolidation of Soft Soils: An Experimental and Theoretical Study," *Géotechnique*, **31**(4), 519 (1981).

Buscall, R., and L. R. White, "The Consolidation of Concentrated Suspensions. Part 1.—The Theory of Sedimentation," *J. Chem. Soc., Faraday Trans.* 1, **83**, 873 (1987).

Bustos, M. C., and F. Concha, "Simulation of Batch Sedimentation with Compression," *AIChE J.*, **34**(5), 859 (1988).

Gibson, R. E., G. L. England, and M. J. L. Hussey, "The Theory of One-Dimensional Consolidation of Saturated Clays," *Géotechnique*, **17**(3), 261 (1967).

Howells, I., K. A. Landman, A. Panjkov, C. Sirakoff, and L. R. White, "Time-Dependent Batch Settling of Flocculated Suspensions," *Appl. Math. Modelling*, **14**, 77 (1990).

Kynch, G. J., "A Theory of Sedimentation," *Trans. Faraday Soc.*, **48**, 166 (1952).

Michaels, A. S., and J. C. Bolger, "Settling Rates and Sediment Volumes of Flocculated Kaolin Suspensions," *Ind. Eng. Chem. Fundam.*, **1**(1), 24 (1962).

Scully, R. W., R. L. Schiffman, H. W. Olsen, and H.-Y. Ko, "Validation of Consolidation Properties of Phosphatic Clay at Very High Void Ratios," *Sedimentation Consolidation Models Predictions and Validation*, Proc. Symp. ASCE Geotechnical Eng. Div., San Francisco, p. 158 (1984).

Shen, C., W. B. Russel, and F. M. Auzerais, "Colloidal Gel Filtration: Experiment and Theory," *AIChE J.*, **40**(11), 1876 (1994).

Theriault, Y., J. H. Masliyah, P. M. Fedorak, R. Vazquez-Duhalt, and M. R. Gray, "The Effect of Chemical, Physical and Enzymatic Treatments on the Dewatering of Tar Sand Tailings," *Fuel*, **74**(9), 1404 (1995).

Manuscript received Jan. 31, 1995, and revision received May 31, 1995.